

---

# VAE with a VampPrior

---

**Jakub M. Tomczak**  
University of Amsterdam  
J.M.Tomczak@uva.nl

**Max Welling**  
University of Amsterdam  
M.Welling@uva.nl

## Abstract

Many different methods to train deep generative models have been proposed in the past. In this paper, we propose to extend the variational auto-encoder (VAE) framework with a new type of prior which we call "Variational Mixture of Posteriors" prior, or VampPrior for short. The VampPrior consists of a mixture distribution (*e.g.*, a mixture of Gaussians) with components given by variational posteriors conditioned on learnable pseudo-inputs. We further extend this prior to a two layer hierarchical model and show that this architecture where prior and posterior are coupled, learns significantly better models. The model also avoids the usual local optima issues that plague VAEs related to useless latent dimensions. We provide empirical studies on three benchmark datasets, namely, MNIST, OMNIGLOT and Caltech 101 Silhouettes, and show that applying the hierarchical VampPrior delivers state-of-the-art results on all three datasets in the unsupervised permutation invariant setting.

## 1 Introduction

Learning generative models that are capable of capturing rich distributions from vast amounts of data like image collections remains one of the major challenges of machine learning. In recent years, different approaches to achieving this goal were proposed by formulating alternative training objectives to the log-likelihood [7, 9, 18] or by utilizing variational inference [1]. The latter approach could be made especially efficient through the application of the *reparameterization trick* resulting in a highly scalable framework now known as the *variational auto-encoders* (VAE) [14, 28]. Various extensions to deep generative models have been proposed that aim to enrich the variational posterior [6, 24, 27, 30, 33, 34]. Recently, it has been noticed that in fact the prior plays a crucial role in mediating between the generative decoder and the variational encoder. Choosing a too simplistic prior like the standard normal distribution could lead to over-regularization and, as a consequence, very poor hidden representations [11].

In this paper, we take a closer look at the regularization term of the variational lower bound inspired by the analysis presented in [21]. Re-formulating the variational lower bound gives two regularization terms: the average entropy of the variational posterior, and the cross-entropy between the averaged (over the training data) variational posterior and the prior. The cross-entropy term can be minimized by setting the prior equal to the average of the variational posteriors over training points. However, this would be computationally very expensive. Instead we propose a new prior that is a *variational mixture of posteriors* prior, or VampPrior for short. Moreover, we present a new two-level VAE that combined with our new prior can learn a very powerful hidden representation.

The contribution of the paper is threefold:

- We follow the line of research of improving the VAE by making the prior more flexible. We propose a new VampPrior, that is a mixture of variational posteriors conditioned on learnable pseudo-data. This allows the variational posterior to learn more a potent latent representation.

- We propose a new two-layered generative VAE model with two layers of stochastic latent variables based on the VampPrior ideas. This architecture effectively avoids the problems of unused latent dimensions.
- We show empirically that our hierarchical VampPrior based VAE achieves state-of-the-art results on three benchmark datasets.

## 2 Variational Auto-Encoder

Let  $\mathbf{x}$  be a vector of  $D$  observable variables and  $\mathbf{z} \in \mathbb{R}^M$  a vector of stochastic latent variables. Further, let  $p_\theta(\mathbf{x}, \mathbf{z})$  be a parametric model of the joint distribution. Given data  $\mathbf{X} = \{\mathbf{x}_1, \dots, \mathbf{x}_N\}$  we typically aim at maximizing the average marginal log-likelihood

$$\frac{1}{N} \ln p(\mathbf{X}) = \frac{1}{N} \sum_{i=1}^N \ln p(\mathbf{x}_i), \quad (1)$$

with respect to parameters. However, when the model is parameterized by a neural network (NN), the optimization could be difficult due to the intractability of the marginal likelihood. One possible fashion of overcoming this issue is to apply *variational inference* and optimize the following lower bound:

$$\mathbb{E}_{\mathbf{x} \sim q(\mathbf{x})} [\ln p(\mathbf{x})] \geq \mathbb{E}_{\mathbf{x} \sim q(\mathbf{x})} [\mathbb{E}_{q_\phi(\mathbf{z}|\mathbf{x})} [\ln p_\theta(\mathbf{x}|\mathbf{z}) + \ln p_\lambda(\mathbf{z}) - \ln q_\phi(\mathbf{z}|\mathbf{x})]] = \mathcal{L}(\phi, \theta, \lambda), \quad (2)$$

where  $q(\mathbf{x}) = \frac{1}{N} \sum_{n=1}^N \delta(\mathbf{x} - \mathbf{x}_n)$  is the empirical distribution,  $q_\phi(\mathbf{z}|\mathbf{x})$  is the *variational posterior* (the *encoder*),  $p_\theta(\mathbf{x}|\mathbf{z})$  is the *generative model* (the *decoder* or the *generator*) and  $p_\lambda(\mathbf{z})$  is the *prior*, and  $\phi, \theta, \lambda$  are their parameters, respectively. There are various ways of optimizing this lower bound but for continuous  $\mathbf{z}$  this could be done efficiently through the *re-parameterization* of  $q_\phi(\mathbf{z}|\mathbf{x})$  [14, 28], which yields a *variational auto-encoder* architecture (VAE). Therefore, during learning we consider a Monte Carlo estimate of the second expectation in (2) using  $L$  sample points:

$$\tilde{\mathcal{L}}(\phi, \theta, \lambda) = \mathbb{E}_{\mathbf{x} \sim q(\mathbf{x})} \left[ \frac{1}{L} \sum_{l=1}^L (\ln p_\theta(\mathbf{x}|\mathbf{z}_\phi^{(l)}) + \ln p_\lambda(\mathbf{z}_\phi^{(l)}) - \ln q_\phi(\mathbf{z}_\phi^{(l)}|\mathbf{x})) \right], \quad (3)$$

where  $\mathbf{z}_\phi^{(l)}$  are sampled from  $q_\phi(\mathbf{z}|\mathbf{x})$  through the re-parameterization trick.

The first component of the objective function can be seen as the expectation of the negative reconstruction error that forces the hidden representation for each data case to be peaked at its specific MAP value. On the contrary, the second and third components constitute a kind of regularization that drives the encoder to match the prior.

Typically, the encoder is assumed to have a diagonal covariance matrix, *i.e.*,  $q_\phi(\mathbf{z}|\mathbf{x}) = \mathcal{N}(\mathbf{z}|\mu_\phi(\mathbf{x}), \text{diag}(\sigma_\phi^2(\mathbf{x})))$ , where  $\mu_\phi(\mathbf{x})$  and  $\sigma_\phi^2(\mathbf{x})$  are parameterized by a NN with weights  $\phi$ , and the prior is expressed using the standard normal distribution,  $p_\lambda(\mathbf{z}) = \mathcal{N}(\mathbf{z}|\mathbf{0}, \mathbf{I})$ . The decoder utilizes a suitable distribution for the data under consideration, *e.g.*, the Bernoulli distribution for binary data or the normal distribution for continuous data, and it is parameterized by a NN with weights  $\theta$ .

## 3 The Variational Mixture of Posteriors Prior

**Motivation** The variational lower-bound consists of two parts, namely, the reconstruction error and the regularization term between the encoder and the prior. However, we can re-write the training objective (2) to obtain two regularization terms instead of one [21]:

$$\mathcal{L}(\phi, \theta, \lambda) = \mathbb{E}_{\mathbf{x} \sim q(\mathbf{x})} [\mathbb{E}_{q_\phi(\mathbf{z}|\mathbf{x})} [\ln p_\theta(\mathbf{x}|\mathbf{z})]] + \mathbb{E}_{\mathbf{x} \sim q(\mathbf{x})} [\mathbb{H}[q_\phi(\mathbf{z}|\mathbf{x})]] - \mathbb{E}_{\mathbf{z} \sim q(\mathbf{z})} [-\ln p_\lambda(\mathbf{z})] \quad (4)$$

where the first component is the negative reconstruction error, the second component is the expectation of the entropy  $\mathbb{H}[\cdot]$  of the variational posterior and the last component is the cross-entropy between the *aggregated posterior* [22] or the *average encoding distribution* [11],  $q(\mathbf{z}) = \frac{1}{N} \sum_{n=1}^N q_\phi(\mathbf{z}|\mathbf{x}_n)$ , and the prior.

The second term of the objective encourages the encoder to have large entropy (*e.g.*, high variance) for every data case. The last term aims at matching the aggregated posterior and the prior. Ideally, the cross-entropy could be zero by simply defining the prior to be  $q(\mathbf{z})$ . However, this choice could potentially lead to overfitting [11, 21]. Moreover, optimizing the recognition model would become very expensive. On the other hand, having a simple prior like the standard normal distribution is known to result in over-regularized models with only few active latent dimensions.

**Idea** In order to minimize the cross-entropy term one could set the prior to the average encoding distribution. However, as mentioned above, this could lead to overfitting and is computationally expensive. In order to overcome both issues we propose to utilize a mixture of variational posteriors with *pseudo-inputs*:

$$p_\lambda(\mathbf{z}) = \frac{1}{K} \sum_{k=1}^K q_\phi(\mathbf{z}|\mathbf{u}_k), \quad (5)$$

where  $K$  is the number of pseudo-inputs, and  $\mathbf{u}_k$  is a  $D$ -dimensional vector we refer to as a *pseudo-input*. The pseudo-inputs are learned during training through backpropagation and can be thought as hyperparameters of the prior,  $\lambda = \{\mathbf{u}_1, \dots, \mathbf{u}_K\}$ . Importantly, the resulting prior is multimodal, thus, it prevents the variational posterior to be over-regularized. On the other hand, incorporating pseudo-inputs prevents from potential overfitting once we pick  $K \ll N$ , which also makes the model less expensive to train. We refer to this prior as the *variational mixture of posteriors prior* (VampPrior).

By coupling the prior with the posterior we entertain fewer parameters and the prior and variational posteriors will at all times “cooperate” during training. This coupling can be easily further studied by inspecting the gradient wrt a single weight  $\phi_i$  for a single data point  $\mathbf{x}$  (see Supplementary Material for details):

$$\frac{\partial}{\partial \phi_i} \tilde{\mathcal{L}}(\mathbf{x}; \phi, \theta, \lambda) = \frac{1}{L} \sum_{l=1}^L \frac{1}{p_\theta(\mathbf{x}|\mathbf{z}_\phi^{(l)})} \frac{\partial}{\partial \mathbf{z}_\phi} p_\theta(\mathbf{x}|\mathbf{z}_\phi^{(l)}) \frac{\partial}{\partial \phi_i} \mathbf{z}_\phi^{(l)} + \quad (6)$$

$$+ \frac{1}{L} \sum_{l=1}^L \left[ \frac{1}{K} \sum_{k=1}^K \left\{ \left( \frac{q_\phi(\mathbf{z}_\phi^{(l)}|\mathbf{x})}{\frac{1}{K} \sum_{k=1}^K q_\phi(\mathbf{z}_\phi^{(l)}|\mathbf{u}_k) q_\phi(\mathbf{z}_\phi^{(l)}|\mathbf{x})} \frac{\partial}{\partial \phi_i} q_\phi(\mathbf{z}_\phi^{(l)}|\mathbf{u}_k) - q_\phi(\mathbf{z}_\phi^{(l)}|\mathbf{u}_k) \frac{\partial}{\partial \phi_i} q_\phi(\mathbf{z}_\phi^{(l)}|\mathbf{x}) \right) \right\} + \quad (7)$$

$$+ \left( \frac{q_\phi(\mathbf{z}_\phi^{(l)}|\mathbf{x})}{\frac{1}{K} \sum_{k=1}^K q_\phi(\mathbf{z}_\phi^{(l)}|\mathbf{u}_k) q_\phi(\mathbf{z}_\phi^{(l)}|\mathbf{x})} \frac{\partial}{\partial \mathbf{z}_\phi} q_\phi(\mathbf{z}_\phi^{(l)}|\mathbf{u}_k) - q_\phi(\mathbf{z}_\phi^{(l)}|\mathbf{u}_k) \frac{\partial}{\partial \mathbf{z}_\phi} q_\phi(\mathbf{z}_\phi^{(l)}|\mathbf{x}) \right) \frac{\partial}{\partial \phi_i} \mathbf{z}_\phi^{(l)} \right] \quad (8)$$

The differences in (7) and (8) are close to 0 as long as  $q_\phi(\mathbf{z}_\phi^{(l)}|\mathbf{x}) \approx q_\phi(\mathbf{z}_\phi^{(l)}|\mathbf{u}_k)$ . Thus, the gradient is influenced by pseudo-inputs that are *dissimilar* to  $\mathbf{x}$ , *i.e.*, if the posterior produces different hidden representations for  $\mathbf{u}_k$  and  $\mathbf{x}$ . In other words, since this has to hold for every training case, the gradient points towards a solution where the variational posterior has high variance. On the contrary, the first part of the objective in (6) causes the posteriors to have low variance and map to different latent explanations for each data case.

## 4 Hierarchical VampPrior Variational Auto-Encoder

**Solving the inactive stochastic latent variable problem** Our VampPrior VAE seems to be an effective remedy against the *inactive stochastic units problem* [3], simply because the prior is designed to be rich and multimodal which prevent the KL term from pulling individual posteriors towards a simple (*e.g.*, standard normal) prior. The *inactive stochastic units problem* is even worse for learning deeper stochastic VAEs (*i.e.*, with multiple layers of stochastic units). The reason might be that stochastic dependencies within a deep generative model are top-down in the generative process and bottom-up in the variational process. As a result, there is less information obtained from real data at the deeper stochastic layers, making them more prone to become regularized towards the prior.

In order to prevent a deep generative model to suffer from the inactive stochastic units problem we propose a new two-layered VAE as follows:

$$q_\phi(\mathbf{z}_1|\mathbf{x}, \mathbf{z}_2) q_\psi(\mathbf{z}_2|\mathbf{x}), \quad (9)$$

while the the generative part is the following:

$$p_{\theta}(\mathbf{x}|\mathbf{z}_1, \mathbf{z}_2) p_{\lambda}(\mathbf{z}_1|\mathbf{z}_2) p(\mathbf{z}_2), \quad (10)$$

with  $p(\mathbf{z}_2)$  given by a VampPrior.

The model is depicted in Figure 1(b).

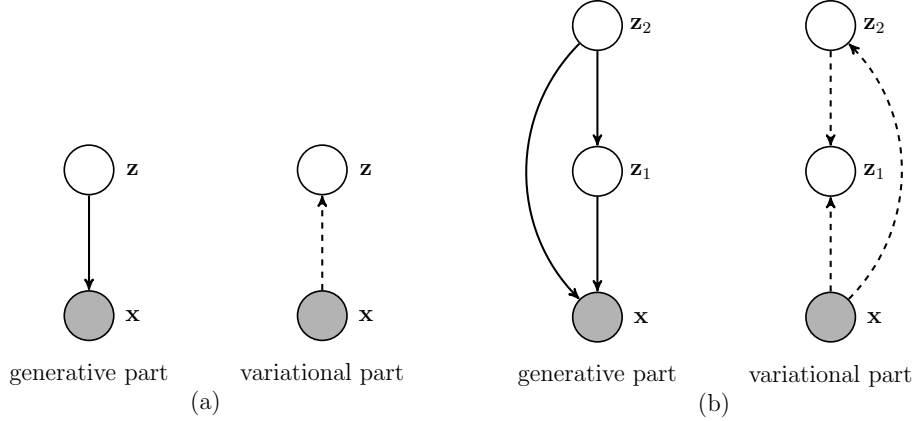


Figure 1: Stochastic dependencies in: (a) a one-layered VAE and (b) a two-layered model. The generative part is denoted by the solid line and the variational part is denoted by the dashed line.

In this model we use normal distributions with diagonal covariance matrices for modeling  $\mathbf{z}_1 \in \mathbb{R}^{M_1}$  and  $\mathbf{z}_2 \in \mathbb{R}^{M_2}$ , parameterized by NNs. The full model is given as:

$$p(\mathbf{z}_2) = \frac{1}{K} \sum_{k=1}^K q_{\psi}(\mathbf{z}_2|\mathbf{u}_k), \quad (11)$$

$$p_{\lambda}(\mathbf{z}_1|\mathbf{z}_2) = \mathcal{N}(\mathbf{z}_1|\mu_{\lambda}(\mathbf{z}_2), \text{diag}(\sigma_{\lambda}^2(\mathbf{z}_2))), \quad (12)$$

$$q_{\phi}(\mathbf{z}_1|\mathbf{x}, \mathbf{z}_2) = \mathcal{N}(\mathbf{z}_1|\mu_{\phi}(\mathbf{x}, \mathbf{z}_2), \text{diag}(\sigma_{\phi}^2(\mathbf{x}, \mathbf{z}_2))), \quad (13)$$

$$q_{\psi}(\mathbf{z}_2|\mathbf{x}) = \mathcal{N}(\mathbf{z}_2|\mu_{\psi}(\mathbf{x}), \text{diag}(\sigma_{\psi}^2(\mathbf{x}))). \quad (14)$$

**Alternative priors** We have motivated the VampPrior by analyzing the variational lower bound. However, one could inquire whether we really need such complicated prior and maybe the proposed two-layered VAE is already sufficiently powerful. In order to answer these questions we further verify three alternative priors:

- the standard Gaussian prior (SG):  $p(\mathbf{z}_2) = \mathcal{N}(\mathbf{0}, \mathbf{I})$ ;
- the mixture of Gaussians prior (MoG):

$$p(\mathbf{z}_2) = \frac{1}{K} \sum_{k=1}^K \mathcal{N}(\mu_k, \text{diag}(\sigma_k^2)),$$

where  $\mu_k \in \mathbb{R}^{M_2}$ ,  $\sigma_k^2 \in \mathbb{R}^{M_2}$  are trainable parameters;

- the VampPrior with a random subset of real training data as non-trainable pseudo-inputs (VampPrior data).

Including the standard prior gives us an answer to the general question if there is even a need for complex priors. Utilizing the mixture of Gaussians verifies whether it is beneficial to couple the prior with the variational posterior. Finally, using a subset of real training images determines to what extent it is useful to introduce trainable pseudo-inputs.

## 5 Experiments

### 5.1 Setting

**Goal** In the experiments we aim at verifying empirically whether the mixture of variational posteriors prior helps VAE to train a representation that better reflects variations in data. Moreover, we want to inspect if our proposition of a two-level generative model performs better than the one-layered model and whether our prior could help to improve the generative performance. In order to fully assess the VampPrior we perform the experiments in the permutation invariant manner, *i.e.*, the decoder and the encoder(s) are parameterized by feed-forward neural networks (MLPs) only.

**Data** We carry out experiments using three benchmark image datasets: MNIST<sup>1</sup>, OMNIGLOT<sup>2</sup> [15], and Caltech 101 Silhouettes<sup>3</sup> [23]. All three datasets contains images of size  $28 \times 28$ .

MNIST consists of hand-written digits split into 60,000 training datapoints and 10,000 test sample points. In order to perform model selection we put aside 10,000 images from the training set. We distinguish between static MNIST with fixed binarization of images<sup>4</sup> [16] and dynamic MNIST with dynamic binarization of data during training as in [29].

OMNIGLOT is a dataset containing 1,623 hand-written characters from 50 various alphabets. Each character is represented by about 20 images that makes the problem very challenging. The dataset is split into 24,345 training datapoints and 8,070 test images. We randomly pick 1,345 training examples for validation. During training we applied dynamic binarization of data similarly to dynamic MNIST.

Caltech 101 Silhouettes contains images representing silhouettes of 101 object classes. Each image is a filled, black polygon of an object on a white background. There are 4,100 training images, 2,264 validation datapoints and 2,307 test examples. The dataset is characterized by a small training sample size and many classes that makes the learning problem ambitious.

**Architecture details** We modeled all distributions using MLPs with two hidden layers of 300 hidden units on MNIST and OMNIGLOT, and one hidden layer of 150 hidden units on Caltech 101 Silhouettes. We utilized the gating mechanism as an element-wise non-linearity [5]. The number of stochastic hidden units was the following: 40 for one-layered VAE and 40 for both  $\mathbf{z}_1$  and  $\mathbf{z}_2$  for the two-layered VAE on MNIST and OMNIGLOT, and 200 for the one-layered VAE and 50 and 200 for  $\mathbf{z}_1$  and  $\mathbf{z}_2$ , respectively, for the two-layered VAE on Caltech 101 Silhouettes.

**Training details** For learning the ADAM algorithm [12] was utilized with the learning rate equal 0.0005 and mini-batches of size 100. Additionally, to boost the generative capabilities of the decoder, we used the *warm-up* for 100 epochs [2]. The weights of neural networks were initialized according to [8]. The early-stopping with a look ahead of 50 iterations was applied. For the VampPrior we used 500 pseudo-inputs for MNIST and Caltech 101 Silhouettes, and 1000 pseudo-inputs for OMNIGLOT. For the VampPrior *data* we used randomly picked training images instead of the learnable pseudo-inputs.

**Evaluation** We compared the one-layered VAE with the VampPrior, VAE ( $L = 1$ ) + VampPrior, and the two-layered VAE with the VampPrior, VAE ( $L = 2$ ) + VampPrior, to other methods with comparable architectures composed of MLPs, such as, Variational Auto-Encoder with the standard normal prior (VAE) [14, 28], VAE with the linear normalizing flow (VAE + NF) [27], Importance Weighted Auto-Encoder (IWAE) [3], VAE with Variational Rényi bound optimization framework (VR-max) [19], Ladder Variational Auto-Encoder (LVAE) [31], VAE with Variational Gaussian Process (VAE + VGP) [34], Auxiliary Deep Generative Model (ADGM) [21], and Cluster-aware DGM that uses no labeled data (CaGeM-0) [20]. In brackets we provide a number of stochastic layers ( $L = 1, 2, 5$ ).

---

<sup>1</sup><http://yann.lecun.com/exdb/mnist/>

<sup>2</sup>We used the pre-processed version of this dataset as in [3]: <https://github.com/yburda/iwae/blob/master/datasets/OMNIGLOT/chardata.mat>.

<sup>3</sup>We used the dataset with fixed split into training, validation and test sets: [https://people.cs.umass.edu/~marlin/data/caltech101\\_silhouettes\\_28\\_split1.mat](https://people.cs.umass.edu/~marlin/data/caltech101_silhouettes_28_split1.mat).

<sup>4</sup><https://github.com/yburda/iwae/tree/master/datasets/BinaryMNIST>

Additionally, we verify the usefulness of the VampPrior in the two-layered VAE by comparing it to the SG prior and the MoG prior on the static MNIST. We performed experiments with the VampPrior *data* on all datasets.

**Implementation** All experiments were run on NVIDIA TITAN X Pascal. The code for our models is available online at [https://github.com/jmtomczak/vae\\_vamprior](https://github.com/jmtomczak/vae_vamprior).

## 5.2 Results

**Quantitative results** We quantitatively evaluate our method using the test marginal log-likelihood (LL) estimated using Importance Sampling with 5,000 sample points [3, 28]. The results are gathered in Table 1, 2, 3 and 4 for static and dynamic MNIST, OMNIGLOT and Caltech 101 Silhouettes, respectively.

Table 1: Test log-likelihood (LL) for static MNIST.

MODEL	LL
VAE ( $L = 1$ ) [3]	-89.05
VAE ( $L = 2$ ) [3]	-87.86
IWAE ( $L = 2$ ) [3]	-85.32
VAE ( $L = 1$ ) + NF [27]	-85.10
VAE ( $L = 2$ ) + SG	-83.59
VAE ( $L = 2$ ) + MoG	-82.77
VAE ( $L = 1$ ) + VampPrior <i>data</i>	-84.90
VAE ( $L = 2$ ) + VampPrior <i>data</i>	-83.41
VAE ( $L = 1$ ) + VampPrior	-83.27
VAE ( $L = 2$ ) + VampPrior	<b>-80.89</b>

Table 2: Test log-likelihood (LL) for dynamic MNIST.

MODEL	LL
VAE ( $L = 1$ ) [3]	-86.76
VAE ( $L = 2$ ) [3]	-85.33
VAE ( $L = 1$ ) + HVI [30]	-85.51
VR-max ( $L = 2$ ) [19]	-83.44
ADGM ( $L = 2$ ) [21]	-82.97
IWAE ( $L = 2$ ) [3]	-82.90
LVAE ( $L = 5$ ) [31]	-81.74
CaGeM-0 ( $L = 2$ ) [20]	-81.60
VAE ( $L = 2$ ) + VGP [34]	-81.32
VAE ( $L = 1$ ) + VampPrior <i>data</i>	-81.30
VAE ( $L = 2$ ) + VampPrior <i>data</i>	-79.41
VAE ( $L = 1$ ) + VampPrior	-80.08
VAE ( $L = 2$ ) + VampPrior	<b>-79.04</b>

Table 3: Test log-likelihood (LL) for OMNIGLOT.

MODEL	LL
VAE ( $L = 1$ ) [3]	-108.11
VAE ( $L = 2$ ) [3]	-107.68
VR-max ( $L = 2$ ) [19]	-103.72
IWAE ( $L = 2$ ) [3]	-103.38
LVAE ( $L = 5$ ) [31]	-102.11
VAE ( $L = 1$ ) + VampPrior <i>data</i>	-106.00
VAE ( $L = 2$ ) + VampPrior <i>data</i>	-101.11
VAE ( $L = 1$ ) + VampPrior	-102.45
VAE ( $L = 2$ ) + VampPrior	<b>-98.88</b>

Table 4: Test log-likelihood (LL) for Caltech 101 Silhouettes.

MODEL	LL
VAE ( $L = 1$ ) [19]	-119.61
IWAE ( $L = 1$ ) [19]	-117.21
VR-max ( $L = 1$ ) [19]	-117.10
VAE ( $L = 1$ ) + VampPrior <i>data</i>	-112.25
VAE ( $L = 2$ ) + VampPrior <i>data</i>	-108.80
VAE ( $L = 1$ ) + VampPrior	-111.79
VAE ( $L = 2$ ) + VampPrior	<b>-105.98</b>

First of all, we notice that the proposed two-layered model is more powerful even with the SG prior (VAE ( $L = 2$ ) + SG) than the standard two-layered VAE, VAE ( $L = 2$ ), see Table 1. Applying the MoG prior results in additional boost of performance. This provides evidence for the usefulness of a multimodal prior. However, the VampPrior *data* gives only slight improvement comparing to the SG prior and because of the application of the fixed training data as the pseudo-inputs it is less flexible

than the MoG. Eventually, coupling the variational posterior with the prior and introducing learnable pseudo-inputs gives the best performance.

In general, an application of the VampPrior improves the performance of the VAE and in the case of two layers of stochastic units it results in state-of-the-art results on all three datasets for models that use MLPs. Moreover, our approach gets very close to the performance of models that utilize convolutional neural networks, such as, the one-layered VAE with the inverse autoregressive flow (IAF) [13] that achieves  $-79.88$  on static MNIST and  $-79.10$  on dynamic MNIST, and the one-layered Variational Lossy Autoencoder (VLAE) that obtains  $-79.03$  on static MNIST and  $-78.53$  on dynamic MNIST. On the other two datasets, which are definitely more challenging, the VLAE performs better than our approach and achieves  $-89.83$  on OMNIGLOT and  $-77.36$  on Caltech 101 Silhouettes. Nevertheless, the performance of VAE ( $L = 2$ ) + VampPrior, which is composed only of MLPs, is very promising and combining it with convolutional operations is left for future work.

An inspection of histograms of the log-likelihoods (see Supplementary Material) shows that the distributions of LL values are heavy-tailed and bimodal for MNIST and Caltech 101 Silhouettes. A possible explanation for such characteristics of the histograms is the existence of many *simple* to represent examples (first mode) and some really *hard* examples (heavy-tail). Comparing our approach to the VAE reveals that VAE + VampPrior is not only better on average but it possesses less examples with high values of LL and more examples with lower LL.

**Qualitative results** The biggest disadvantage of the VAE is that it tends to produce blurry images [17]. We noticed this effect in images generated by VAE (see Supplementary Material). Moreover, the standard VAE produced some digits that are hard to interpret, blurry characters and very noisy silhouettes. The supremacy of VAE ( $L = 2$ ) + VampPrior is visible not only in LL values but in image generations as well. Images generated by VAE ( $L = 2$ ) + VampPrior are sharper. Additionally, its reconstructions contain more details than the ones given by VAE (see Supplementary Material).

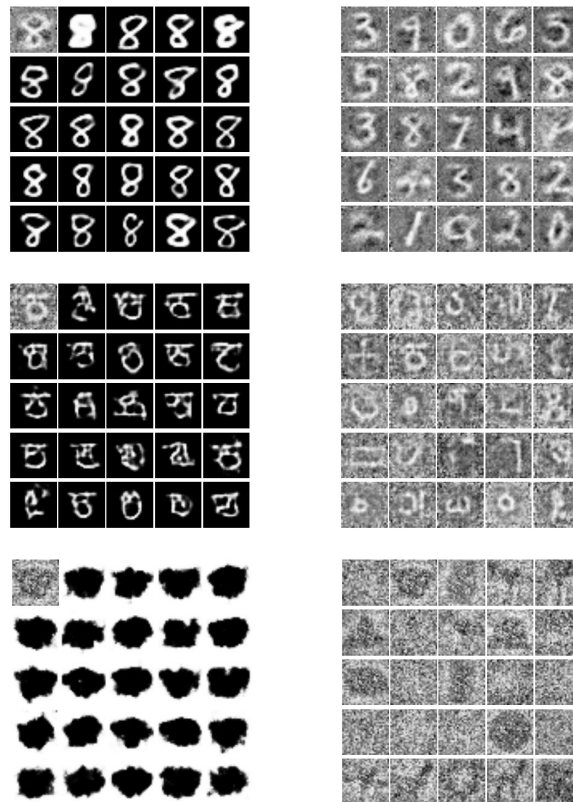


Figure 2: (left column) Images generated by VAE ( $L = 2$ ) + VampPrior for chosen pseudo-input in the left top corner. (right column) Images represent trained pseudo-inputs for MNIST, OMNIGLOT, and Caltech 101 Silhouettes, respectively.

We also examine what the pseudo-inputs represent at the end of the training process (see Figure 2). Interestingly, trained pseudo-inputs are prototypical objects (digits, characters, silhouettes). Moreover, images generated for a chosen pseudo-input show that the model encodes a high variety of different features such as shapes, thickness and curvature for a single pseudo-input. This means that the model is not just memorizing the data-cases.

## 6 Related work

The VAE is a probabilistic latent variable model that is usually trained with a very simple prior, *i.e.*, the standard normal prior. In [25] a Dirichlet process prior using a stick-breaking process was proposed, while [10] proposed a nested Chinese Restaurant Process. These priors indeed enrich the generative capabilities of the VAE, however, they require sophisticated learning methods and tricks to be trained successfully. A different approach is to use an autoregressive prior [4] that applies the IAF to random noise. This approach gives very promising results and allows to build rich representations. Nevertheless, the authors of [4] combine their prior with convolutional networks and an autoregressive decoder that makes it difficult to assess the real contribution of the autoregressive prior to the generative model.

Obviously, the quality of generated images are dependent on the decoder architecture. One way of improving generative capabilities of the decoder is to use an infinite mixture of probabilistic component analyzers [32], which is equivalent to a rank-one covariance matrix. A more appealing approach would be to use cutting-edge deep autoregressive density estimators that utilize recurrent neural networks [26] or convolutional networks [35]. However, there is a threat that a too flexible decoder could discard hidden representations completely, turning the encoder to be useless [4]. Nevertheless, incorporating these models to our two-layered generative model with the VampPrior is very appealing and we leave verifying it for future research.

## 7 Conclusion

In this paper, we followed the line of thinking that the prior is a critical element to improve deep generative models, and in particular VAEs. We proposed a new prior that is expressed as a mixture of variational posteriors. In order to limit the capacity of the prior we introduced learnable pseudo-inputs as hyper-parameters of the prior, the number of which can be chosen freely. Further, we formulated a new two-level generative model based on this VampPrior. We showed empirically that applying our prior can indeed increase the performance of the proposed generative model and successfully overcome the problem of inactive stochastic latent variables, which is particularly challenging for generative models with multiple layers of stochastic latent variables. As a result, we achieved state-of-the-art results in the unsupervised permutation invariant setting on three benchmark datasets. Additionally, generations and reconstructions obtained from the two-layered VAE with the VampPrior are of better quality than the ones achieved by the standard VAE.

We believe that it is worthwhile to further pursue the line of the research presented in this paper. Here we applied our prior to image data but it would be interesting to see how it behaves on text or sound, where the sequential aspect plays a crucial role. We have already pointed out that combining the VampPrior VAE with convolutional nets and powerful autoregressive density estimators could give a further boost in performance. Last but not least, it would be interesting to utilize a normalizing flow within the VampPrior VAE. However, we leave investigating these issues for future work.

## Acknowledgments

The research conducted by Jakub M. Tomczak was funded by the European Commission within the Marie Skłodowska-Curie Individual Fellowship (Grant No. 702666, "Deep learning and Bayesian inference for medical imaging").

## References

- [1] D. M. Blei, A. Kucukelbir, and J. D. McAuliffe. Variational inference: A review for statisticians. *Journal of the American Statistical Association*, 2017.
- [2] S. R. Bowman, L. Vilnis, O. Vinyals, A. M. Dai, R. Jozefowicz, and S. Bengio. Generating sentences from a continuous space. *arXiv preprint arXiv:1511.06349*, 2016.
- [3] Y. Burda, R. Grosse, and R. Salakhutdinov. Importance weighted autoencoders. *arXiv preprint arXiv:1509.00519*, 2015.
- [4] X. Chen, D. P. Kingma, T. Salimans, Y. Duan, P. Dhariwal, J. Schulman, I. Sutskever, and P. Abbeel. Variational Lossy Autoencoder. *arXiv preprint arXiv:1611.02731*, 2016.
- [5] Y. N. Dauphin, A. Fan, M. Auli, and D. Grangier. Language Modeling with Gated Convolutional Networks. *arXiv preprint arXiv:1612.08083*, 2016.
- [6] L. Dinh, D. Krueger, and Y. Bengio. NICE: Non-linear independent components estimation. *arXiv preprint arXiv:1410.8516*, 2014.
- [7] G. Dziugaite, D. Roy, and Z. Ghahramani. Training generative neural networks via maximum mean discrepancy optimization. *UAI*, pages 258–267, 2015.
- [8] X. Glorot and Y. Bengio. Understanding the difficulty of training deep feedforward neural networks. *AISTATS*, 9:249–256, 2010.
- [9] I. Goodfellow, J. Pouget-Abadie, M. Mirza, B. Xu, D. Warde-Farley, S. Ozair, A. Courville, and Y. Bengio. Generative adversarial nets. *NIPS*, pages 2672–2680, 2014.
- [10] P. Goyal, Z. Hu, X. Liang, C. Wang, and E. Xing. Nonparametric Variational Auto-encoders for Hierarchical Representation Learning. *arXiv preprint arXiv:1703.07027*, 2017.
- [11] M. D. Hoffman and M. J. Johnson. ELBO surgery: yet another way to carve up the variational evidence lower bound. *NIPS Workshop: Advances in Approximate Bayesian Inference*, 2016.
- [12] D. Kingma and J. Ba. Adam: A method for stochastic optimization. *arXiv preprint arXiv:1412.6980*, 2014.
- [13] D. P. Kingma, T. Salimans, R. Jozefowicz, X. Chen, I. Sutskever, and M. Welling. Improved variational inference with inverse autoregressive flow. *NIPS*, pages 4743–4751, 2016.
- [14] D. P. Kingma and M. Welling. Auto-encoding variational bayes. *arXiv preprint arXiv:1312.6114*, 2013.
- [15] B. M. Lake, R. Salakhutdinov, and J. B. Tenenbaum. Human-level concept learning through probabilistic program induction. *Science*, 350(6266):1332–1338, 2015.
- [16] H. Larochelle and I. Murray. The Neural Autoregressive Distribution Estimator. *AISTATS*, 2011.
- [17] A. B. L. Larsen, S. K. Sønderby, H. Larochelle, and O. Winther. Autoencoding beyond pixels using a learned similarity metric. *ICML*, 2016.
- [18] Y. Li, K. Swersky, and R. S. Zemel. Generative moment matching networks. *ICML*, pages 1718–1727, 2015.
- [19] Y. Li and R. E. Turner. Rényi Divergence Variational Inference. *NIPS*, pages 1073–1081, 2016.
- [20] L. Maaløe, M. Fraccaro, and O. Winther. Semi-supervised generation with cluster-aware generative models. *arXiv preprint arXiv:1704.00637*, 2017.
- [21] L. Maaløe, C. K. Sønderby, S. K. Sønderby, and O. Winther. Auxiliary deep generative models. *ICML*, pages 1445–1453, 2016.
- [22] A. Makhzani, J. Shlens, N. Jaitly, I. Goodfellow, and B. Frey. Adversarial autoencoders. *arXiv preprint arXiv:1511.05644*, 2015.
- [23] B. Marlin, K. Swersky, B. Chen, and N. Freitas. Inductive principles for Restricted Boltzmann Machine learning. *AISTATS*, pages 509–516, 2010.
- [24] E. Nalisnick, L. Hertel, and P. Smyth. Approximate Inference for Deep Latent Gaussian Mixtures. *NIPS Workshop: Bayesian Deep Learning*, 2016.
- [25] E. Nalisnick and P. Smyth. Stick-Breaking Variational Autoencoders. *arXiv preprint arXiv:1605.06197*, 2016.

- [26] A. V. d. Oord, N. Kalchbrenner, and K. Kavukcuoglu. Pixel Recurrent Neural Networks. *ICML*, pages 1747–1756, 2016.
- [27] D. J. Rezende and S. Mohamed. Variational inference with normalizing flows. *arXiv preprint arXiv:1505.05770*, 2015.
- [28] D. J. Rezende, S. Mohamed, and D. Wierstra. Stochastic Backpropagation and Approximate Inference in Deep Generative Models. *ICML*, pages 1278–1286, 2014.
- [29] R. Salakhutdinov and I. Murray. On the quantitative analysis of deep belief networks. *ICML*, pages 872–879, 2008.
- [30] T. Salimans, D. Kingma, and M. Welling. Markov chain monte carlo and variational inference: Bridging the gap. *ICML*, pages 1218–1226, 2015.
- [31] C. K. Sønderby, T. Raiko, L. Maaløe, S. K. Sønderby, and O. Winther. Ladder variational autoencoders. *NIPS*, pages 3738–3746, 2016.
- [32] S. Suh and S. Choi. Gaussian Copula Variational Autoencoders for Mixed Data. *arXiv preprint arXiv:1604.04960*, 2016.
- [33] J. M. Tomczak and M. Welling. Improving Variational Auto-Encoders using Householder Flow. *NIPS Workshop: Bayesian Deep Learning*, 2016.
- [34] D. Tran, R. Ranganath, and D. M. Blei. The variational Gaussian process. *arXiv preprint arXiv:1511.06499*, 2015.
- [35] A. van den Oord, N. Kalchbrenner, L. Espeholt, O. Vinyals, A. Graves, and K. Kavukcuoglu. Conditional image generation with PixelCNN decoders. *NIPS*, pages 4790–4798, 2016.

## 8 SUPPLEMENTARY MATERIAL

### 8.1 Details on the gradient calculation in Eq. 8

Let us recall the objective function for single datapoint  $\mathbf{x}_*$  using  $L$  Monte Carlo sample points:

$$\tilde{\mathcal{L}}(\mathbf{x}_*; \phi, \theta, \lambda) = \frac{1}{L} \sum_{l=1}^L \left[ \ln p_\theta(\mathbf{x}_* | \mathbf{z}_\phi^{(l)}) \right] + \frac{1}{L} \sum_{l=1}^L \left[ \ln \frac{1}{K} \sum_{k=1}^K q_\phi(\mathbf{z}_\phi^{(l)} | \mathbf{u}_k) - \ln q_\phi(\mathbf{z}_\phi^{(l)} | \mathbf{x}_*) \right]. \quad (15)$$

We are interested in calculating gradient with respect to a single parameter  $\phi_i$ . We can split the gradient into two parts:

$$\begin{aligned} \frac{\partial}{\partial \phi_i} \tilde{\mathcal{L}}(\mathbf{x}_*; \phi, \theta, \lambda) &= \frac{\partial}{\partial \phi_i} \underbrace{\frac{1}{L} \sum_{l=1}^L \left[ \ln p_\theta(\mathbf{x}_* | \mathbf{z}_\phi^{(l)}) \right]}_{(*)} \\ &\quad + \frac{\partial}{\partial \phi_i} \underbrace{\frac{1}{L} \sum_{l=1}^L \left[ \ln \frac{1}{K} \sum_{k=1}^K q_\phi(\mathbf{z}_\phi^{(l)} | \mathbf{u}_k) - \ln q_\phi(\mathbf{z}_\phi^{(l)} | \mathbf{x}_*) \right]}_{(**)} \end{aligned} \quad (16)$$

Calculating the gradient separately for both  $(*)$  and  $(**)$  yields:

$$\begin{aligned} \frac{\partial}{\partial \phi_i} (*) &= \frac{\partial}{\partial \phi_i} \frac{1}{L} \sum_{l=1}^L \left[ \ln p_\theta(\mathbf{x}_* | \mathbf{z}_\phi^{(l)}) \right] \\ &= \frac{1}{L} \sum_{l=1}^L \frac{1}{p_\theta(\mathbf{x}_* | \mathbf{z}_\phi^{(l)})} \frac{\partial}{\partial \mathbf{z}_\phi} p_\theta(\mathbf{x}_* | \mathbf{z}_\phi^{(l)}) \frac{\partial}{\partial \phi_i} \mathbf{z}_\phi^{(l)} \end{aligned} \quad (17)$$

$$\begin{aligned} \frac{\partial}{\partial \phi_i} (**) &= \frac{\partial}{\partial \phi_i} \frac{1}{L} \sum_{l=1}^L \left[ \ln \frac{1}{K} \sum_{k=1}^K q_\phi(\mathbf{z}_\phi^{(l)} | \mathbf{u}_k) - \ln q_\phi(\mathbf{z}_\phi^{(l)} | \mathbf{x}_*) \right] \\ &\quad [\text{Short-hand notation: } q_\phi(\mathbf{z}_\phi^{(l)} | \mathbf{x}_*) \triangleq q_\phi^*, \quad q_\phi(\mathbf{z}_\phi^{(l)} | \mathbf{u}_k) \triangleq q_\phi^k] \\ &= \frac{1}{L} \sum_{l=1}^L \left[ \frac{1}{\frac{1}{K} \sum_{k=1}^K q_\phi^k} \left( \frac{\partial}{\partial \phi_i} \frac{1}{K} \sum_{k=1}^K q_\phi^k + \frac{\partial}{\partial \mathbf{z}_\phi} \left( \frac{1}{K} \sum_{k=1}^K q_\phi^k \right) \frac{\partial}{\partial \phi_i} \mathbf{z}_\phi^{(l)} \right) + \right. \\ &\quad \left. - \frac{1}{q_\phi^*} \left( \frac{\partial}{\partial \phi_i} q_\phi^* + \frac{\partial}{\partial \mathbf{z}_\phi} q_\phi^* \frac{\partial}{\partial \phi_i} \mathbf{z}_\phi^{(l)} \right) \right] \\ &= \frac{1}{L} \sum_{l=1}^L \left[ \frac{1}{\frac{1}{K} \sum_{k=1}^K q_\phi^k q_\phi^*} \left( \frac{1}{K} \sum_{k=1}^K q_\phi^* \frac{\partial}{\partial \phi_i} q_\phi^k + \left( \frac{1}{K} \sum_{k=1}^K q_\phi^* \frac{\partial}{\partial \mathbf{z}_\phi} q_\phi^k \right) \frac{\partial}{\partial \phi_i} \mathbf{z}_\phi^{(l)} \right) + \right. \\ &\quad \left. - \frac{1}{\frac{1}{K} \sum_{k=1}^K q_\phi^k q_\phi^*} \left( \frac{1}{K} \sum_{k=1}^K q_\phi^k \frac{\partial}{\partial \phi_i} q_\phi^* + \frac{1}{K} \sum_{k=1}^K q_\phi^k \frac{\partial}{\partial \mathbf{z}_\phi} q_\phi^* \frac{\partial}{\partial \phi_i} \mathbf{z}_\phi^{(l)} \right) \right] \\ &= \frac{1}{L} \sum_{l=1}^L \left[ \frac{1}{\frac{1}{K} \sum_{k=1}^K q_\phi^k q_\phi^*} \frac{1}{K} \sum_{k=1}^K \left\{ \left( q_\phi^* \frac{\partial}{\partial \phi_i} q_\phi^k - q_\phi^k \frac{\partial}{\partial \phi_i} q_\phi^* \right) + \right. \right. \\ &\quad \left. \left. + \left( q_\phi^* \frac{\partial}{\partial \mathbf{z}_\phi} q_\phi^k - q_\phi^k \frac{\partial}{\partial \mathbf{z}_\phi} q_\phi^* \right) \frac{\partial}{\partial \phi_i} \mathbf{z}_\phi^{(l)} \right\} \right] \end{aligned} \quad (18)$$

For comparison, the gradient of (\*\*) for the standard normal prior  $p_\lambda(\mathbf{z}) = \mathcal{N}(\mathbf{z}|\mathbf{0}, \mathbf{I})$  is the following:

$$\begin{aligned}
& \frac{\partial}{\partial \phi_i} \frac{1}{L} \sum_{l=1}^L \ln p_\lambda(\mathbf{z}_\phi^{(l)}) - \ln q_\phi(\mathbf{z}_\phi^{(l)}|\mathbf{x}_*) = \\
& \text{[Short-hand notation: } q_\phi(\mathbf{z}_\phi^{(l)}|\mathbf{x}_*) \triangleq q_\phi^*, \quad p_\lambda(\mathbf{z}_\phi^{(l)}) \triangleq p_\lambda] \\
& = \frac{1}{L} \sum_{l=1}^L \left[ \frac{1}{p_\lambda} \frac{\partial}{\partial \mathbf{z}_\phi} p_\lambda \frac{\partial}{\partial \phi_i} \mathbf{z}_\phi^{(l)} - \frac{1}{q_\phi^*} \left( \frac{\partial}{\partial \phi_i} q_\phi^* + \frac{\partial}{\partial \mathbf{z}_\phi} q_\phi^* \frac{\partial}{\partial \phi_i} \mathbf{z}_\phi^{(l)} \right) \right] \\
& = \frac{1}{L} \sum_{l=1}^L \left[ -\frac{1}{q_\phi^*} \frac{\partial}{\partial \phi_i} q_\phi^* + \frac{1}{p_\lambda q_\phi^*} \left( q_\phi^* \frac{\partial}{\partial \mathbf{z}_\phi} p_\lambda - p_\lambda \frac{\partial}{\partial \phi_i} q_\phi^* \right) \frac{\partial}{\partial \phi_i} \mathbf{z}_\phi^{(l)} \right] \tag{19}
\end{aligned}$$

We notice that in (18) if  $q_\phi^* \approx q_\phi^k$  for some  $k$ , then the differences  $(q_\phi^* \frac{\partial}{\partial \phi_i} q_\phi^k - q_\phi^k \frac{\partial}{\partial \phi_i} q_\phi^*)$  and  $(q_\phi^* \frac{\partial}{\partial \mathbf{z}_\phi} q_\phi^k - q_\phi^k \frac{\partial}{\partial \mathbf{z}_\phi} q_\phi^*)$  are close to 0. Hence, the gradient points into an average of all dissimilar pseudo-inputs contrary to the gradient of the standard normal prior in (19) that pulls always towards  $\mathbf{0}$ . As a result, the encoder is trained so that to have large variance because it is attracted by all dissimilar points and due to this fact it assigns separate regions in the latent space to each datapoint. This effect should help the decoder to decode a hidden representation to an image much easier.

## 8.2 Additional results

The generated images are presented in Figure 3. Images generated by VAE ( $L = 2$ ) + VampPrior are more realistic and sharper than the ones given by the vanilla VAE.

The reconstructions from test images are presented in Figure 4. At first glance the reconstructions of VAE and VAE ( $L = 2$ ) + VampPrior look similarly, however, our approach provides more details and the reconstructions are sharper. This is especially visible in the case of OMNIGLOT (middle row in Figure 4) where VAE is incapable to reconstruct small circles while our approach does in most cases.

The histograms of the log-likelihood per test example are presented in Figure 5. We notice that all histograms characterize a heavy-tail indicating existence of examples that are hard to represent. However, taking a closer look at the histograms for VAE ( $L = 2$ ) + VampPrior reveals that there are less hard examples comparing to the standard VAE.

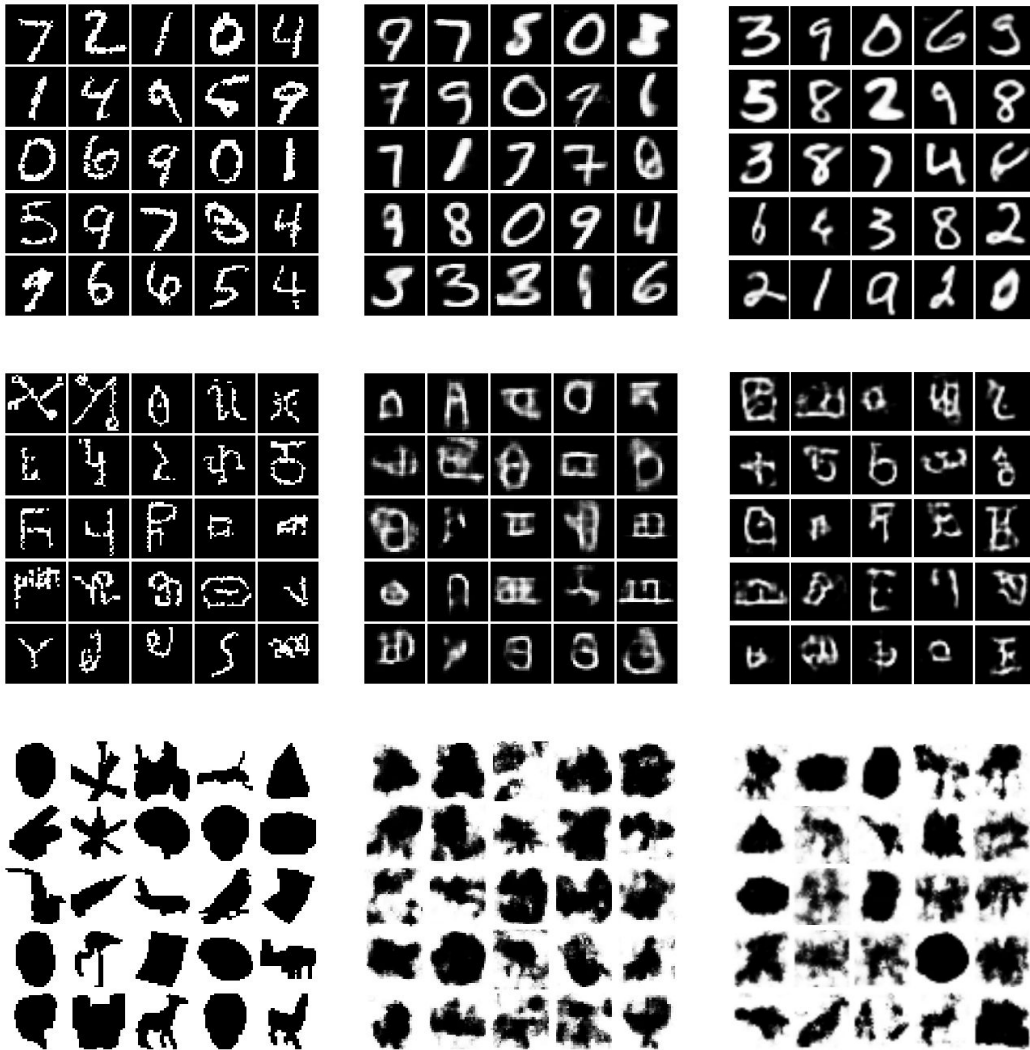


Figure 3: Real images from test sets (*left*), images generated by the vanilla VAE (*middle*) and the VAE ( $L = 2$ ) + VampPrior (*right*).

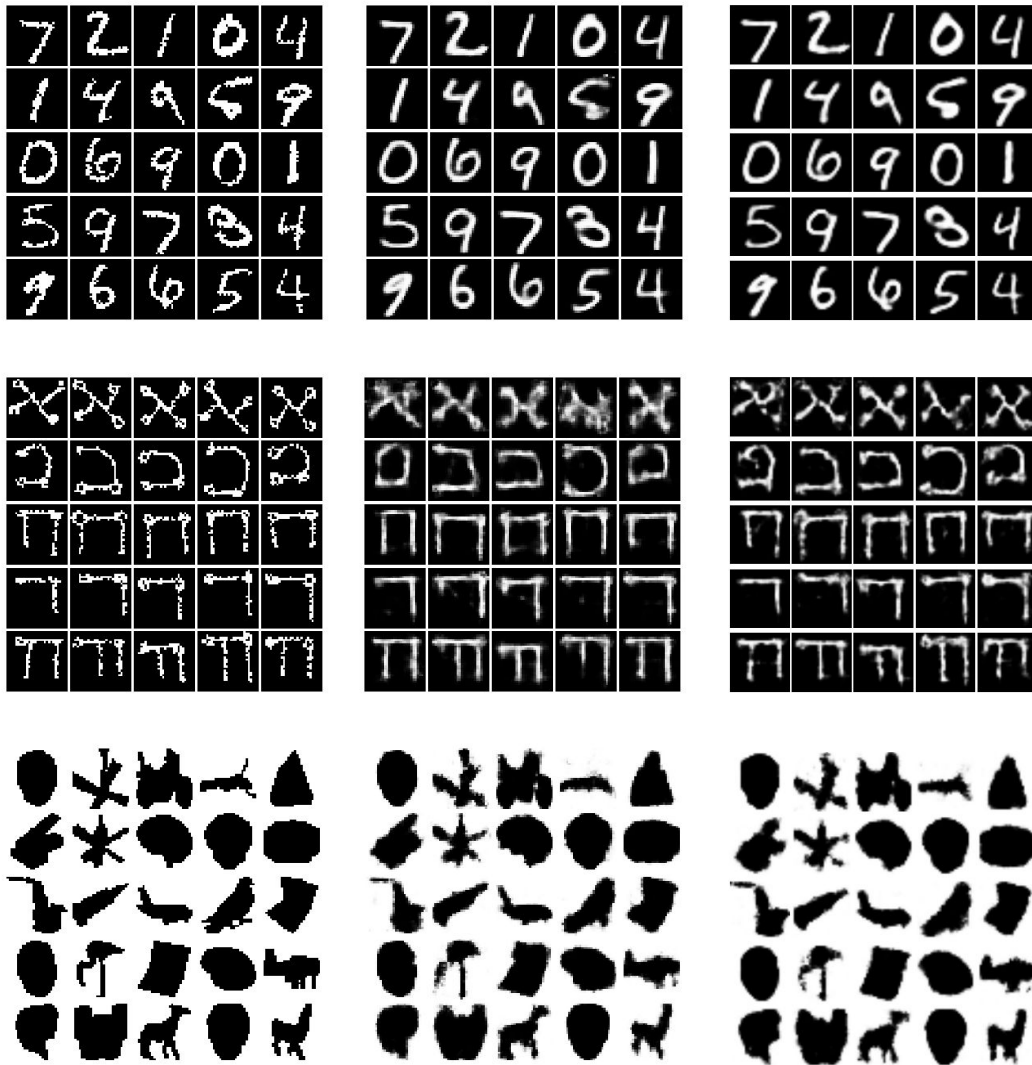


Figure 4: Real images from test sets (*left*), reconstructions given by the vanilla VAE (*middle*) and VAE ( $L = 2$ ) + VampPrior (*right*).

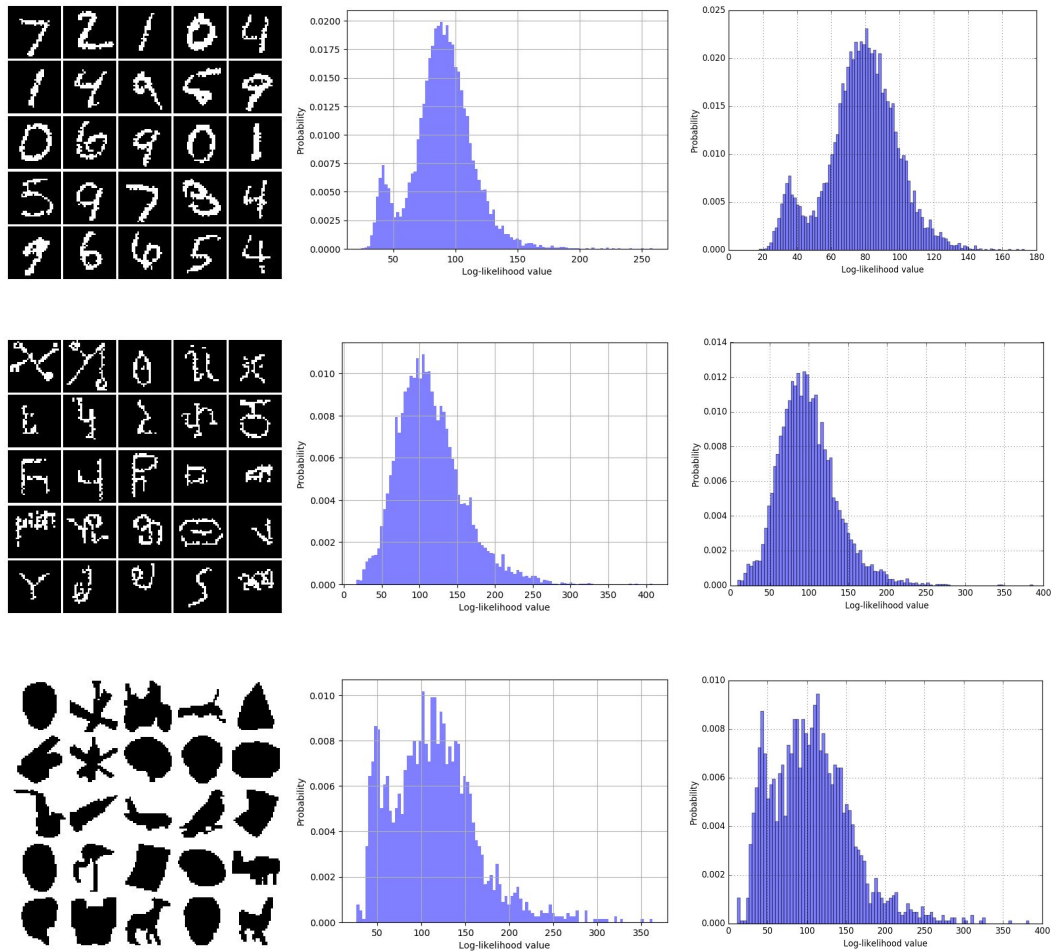


Figure 5: Histograms of test log-likelihoods calculated on MNIST (*top row*), OMNIGLOT (*middle row*) and Caltech101Silhouettes (*bottom row*) for the vanilla VAE (*middle column*) and VAE ( $L = 2$ ) + VampPrior (*right column*).